

Evaluating a natural gas pipeline steel for blended hydrogen service

May L. Martin ^{*}, Matthew Connolly, Zachary N. Buck, Peter E. Bradley, Damian Lauria, Andrew J. Slifka

Applied Chemicals and Materials Division, Material Measurement Laboratory, National Institute of Standards and Technology, Boulder, CO, 80305, USA

ABSTRACT

An X70 natural gas pipeline steel that is being considered for blended natural gas/hydrogen gas service was evaluated in a high-pressure hydrogen gas environment. Fracture toughness testing and fatigue crack growth rate testing were conducted according to ASTM standards and the results are presented in the context of ASME B31.12 qualification. While a reduction in fracture toughness was observed, the fracture toughness and fatigue behavior were within acceptable bounds for hydrogen service.



1. Introduction

New research activity regarding the compatibility of natural gas pipeline infrastructures with hydrogen gas is due to an active interest by governments and industry in blending 5–15% hydrogen gas with natural gas. Hydrogen and natural gas blending was even specifically mentioned in a press release about a collaboration between US and Dutch governments on hydrogen infrastructure technologies (Collaboration Between the, 2020). Multiple advantages of blending have been discussed and include energy storage of the increased output from green energy technologies, and cheaper transportation of hydrogen gas for fuel cell use (Melaina et al., 2013). The most recent focus has been on the use of blending as a method of reducing the amount of carbon in natural gas applications, without significantly reducing energy density or completely overhauling the system (Dept. of Energy and HyBLE, 2021). While the presence of hydrogen mixed in with methane is not novel, as manufactured or synthetic gas historically contained as much as 50% hydrogen in the mix (Melaina and Grasman, 2016), safety concerns still remain.

One of the main safety concerns with the addition of hydrogen into steel pipeline systems is hydrogen embrittlement. When hydrogen atoms enter the metal matrix, they can cause a drastic reduction in the ductility of steel, also commonly resulting in a reduction in fracture toughness and a reduction in fatigue lifetime (Martin et al., 2020). Although certain alloys, such as austenitic stainless steels are more resistant to hydrogen effects, pipeline steels tend to be ferritic due to cost considerations and are particularly vulnerable to reductions in fatigue lifetime (San Marchi et al., 2010; Slifka et al., 2014a, 2015; Ronevich et al., 2016). While much of the research on hydrogen effects on fracture

toughness and fatigue are performed in pure hydrogen, studies of mixtures of methane and hydrogen gas show that small percentages of hydrogen can have dramatic effects on fracture toughness (Nguyen et al., 2020) and fatigue crack growth rates (Meng et al., 2017; Chandra et al., 2021) of pipeline steels. For simplicity, testing in pure hydrogen gas is generally performed, as it constitutes a “worse-case scenario” for the effects on mechanical properties.

There are only a limited number of laboratories with the capability for *in situ* gaseous hydrogen testing, which can be required by the ASME B31.12–2019 code for certifying pipeline steels for hydrogen service (as well as the API 5 L code) (Hydrogen Piping and, 2020). Many companies opt for “Option A”, which requires Charpy testing (in air) within a specific energy range. However, to compensate for the lack of testing in hydrogen, there are many safety factor requirements that are further imposed for the use of materials certified in this manner. This results in overdesign of the pipelines, which can be costly. “Option B” requires testing in hydrogen, including the determination of fracture toughness, fatigue crack growth rate (FCGR), and stress intensity factor threshold. Each of these tests must show results that are better than the minimum acceptable values stated within the standard under conditions similar to the expected operating conditions of the material, such as service pressure of hydrogen. While only a limited number of laboratories are capable of testing in gaseous hydrogen, even fewer perform *in situ* tests of stress intensity threshold. Additionally, the constant-displacement stress intensity threshold measurement has been shown to give non-conservative results when the plasticity accompanying the fracture is large. Materials which are suitable for hydrogen service will have large amounts of plasticity, as this plasticity gives rise to greater fracture resistance; so constant-displacement stress intensity factor threshold

* Corresponding author.

E-mail address: may.martin@nist.gov (M.L. Martin).

measurements are especially likely to give non-conservative assessments of hydrogen behavior (Nibur et al., 2013; Dadfarnia et al., 2010). For these reasons, FCGR and fracture toughness tests are less likely to be overly- or under-conservative, so these tests are most useful to assess materials for hydrogen/natural gas service. As a result, there are discussions within the ASME B31.12 code committee about removing the stress intensity threshold testing requirement from future drafts of the standard and simply requiring FCGR and ASME E1820 fracture toughness testing (Slifka and Stalheim, 2021).

Commercially obtained X70 pipeline steel that is of interest for use in blended natural gas/H₂ gas service is being tested for certification. Fracture toughness and FCGR testing were performed in hydrogen gas and the test results are presented in the context of ASME B31.12 qualification. Fracture toughness testing was performed in accordance with ASTM E1820-20 (Standard Test Method for, 2019) and FCGR testing was done in accordance with ASTM E647-15 (Standard Test Method for, 2017). It is important to note that this paper is not presenting intrinsic materials parameters, but the relative degradation of performance due to the hydrogen environment.

2. Material and testing methods

Specimens were cut from a section of X70 pipe that has not seen service but was from a lot prepared for natural gas service. The pipe had a wall thickness of 21.5 mm. Chemistry for the steel is shown in Table 1. Cubes were sectioned and mounted in epoxy to examine the three directions of the pipe (rolling/longitudinal RD, transverse/circumferential TD, and through-thickness TT). A section was also taken to examine the through thickness of the seam weld. The specimens were polished and etched with a 2% nital (nitric acid in methanol) solution for optical microscopy analysis and scanning electron microscopy (SEM) imaging analysis. Specimens were then polished to a mirror finish with 0.05 µm colloidal silica for electron backscattered (EBSD) analysis in an SEM. Grain size and microstructural texture were derived from the crystal orientation data.

This X70 pipeline steel shows a ferritic/pearlitic microstructure with ~15% pearlite, Fig. 1. There is a clear banded microstructure associated with rolling, evident from the pearlite grains in fine bands along the rolling direction. The pearlite grains consist of very fine cementite plates in a ferrite matrix, usually in a band that is a single grain wide, and several grains long in the rolling direction, Fig. 2. Grains are slightly elongated, and the texture is strongly <101> in the rolling direction with more of a <111> texture in the transverse direction, Fig. 2. The average grain size across all three planes is 4.9 µm. The grain size homogeneity factor, defined as the ratio of the grain size of the 20% area fraction distribution (the D₂₀ grain size) to the average grain size, is 2.7 in the both the TD and RD planes, and 6.0 in the TT plane. This suggests higher grain size homogeneity in the TD and RD directions than in the TT direction.

The weld specimens were cut from a longitudinal (“seam”) weld. The weld was a commercial induction weld. The weld is composed of two beads, one on either side of the plate, Fig. 3. The macrostructure clearly shows the results of solidification, with long prior austenite grain structures radiating from the root to the surface of the bead consisting of fine Widmanstätten ferrite plates with allotriomorphic ferrite along the prior austenite grain boundaries. On both sides of both weld beads, there are wide (~2 mm) heat affected zones (HAZs).

Fracture toughness (J_Q) tests were performed according to ASTM E1820 (Standard Test Method for, 2019) on side-grooved compact tension (CT) specimens in air and in 10 MPa ultra-pure grade hydrogen gas

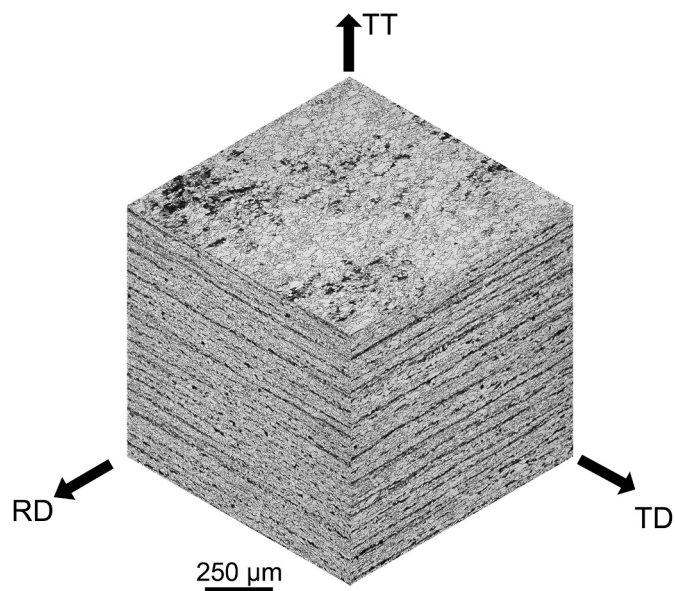


Fig. 1. Microstructure of X70 steel, showing the 3 directions in the steel plate. Etched with 2% nital solution.

(99.999% pure). Specimens were machined from the pipe wall according to the ASTM E1820 standard (Standard Test Method for, 2019) with a nominal width (W) of 40.6 mm, a thickness (B) of 20 mm, and were side-grooved to have a net thickness (B_n) of 16 mm. Specimens were oriented with the crack direction in the rolling direction for the base metal and with the crack to the side of the weld beads to capture the heat affected zone (HAZ), as well as weld metal, for the seam weld metal. This means the crack plane is the plane normal to TD. The crack plane for the HAZ specimens are marked with the yellow dashed line in Fig. 3, and a schematic of the CT specimen position relative to the weld bead can be found in Fig. 4 of Ref. (Slifka et al., 2015). This geometry best captures the hoop stresses on the pipe, which are expected to be the largest. The fracture toughness was determined from J-R curves, which were measured using a crack mouth opening displacement (CMOD) sensor and the compliance method to determine crack extension. Fracture surfaces from the fracture toughness specimens were examined in an SEM operated at 30 kV.

Fatigue crack growth rate (FCGR) tests were performed on CT specimens without side grooves in 10 MPa ultra-pure grade hydrogen gas (99.999% pure) from the base metal (3 specimens) and the weld (3 specimens). The CT specimens for FCGR tests had a thickness (B) of 9.45 mm. The base metal fatigue specimens were cut with identical orientations to the fracture toughness specimens, with the cracking direction in the rolling direction. For the weld specimens, this orientation results in the crack following the center of the two weld beads as marked with the red solid line in Fig. 3, with the crack propagating in the rolling direction (into the page in Fig. 3). Pre-cracking was performed in air at room temperature with load ratio R = 0.1 and loading frequency of 15 Hz. These specimens were run simultaneously in a chain, see (Drexler et al., 2016) for details on the experimental setup, such that they all experienced the identical gaseous environment during mechanical loading. Fatigue tests were conducted with R = 0.5 at a loading frequency of 1 Hz.

Table 1
Composition of X70 steel in this study in mass %. Remainder Fe.

C	Si	Mn	P	S	Cu	Al	Cr	Ni	Nb	Ti	N
0.084	0.35	1.75	0.014	0.0007	0.03	0.031	0.04	0.04	0.045	0.014	0.0039

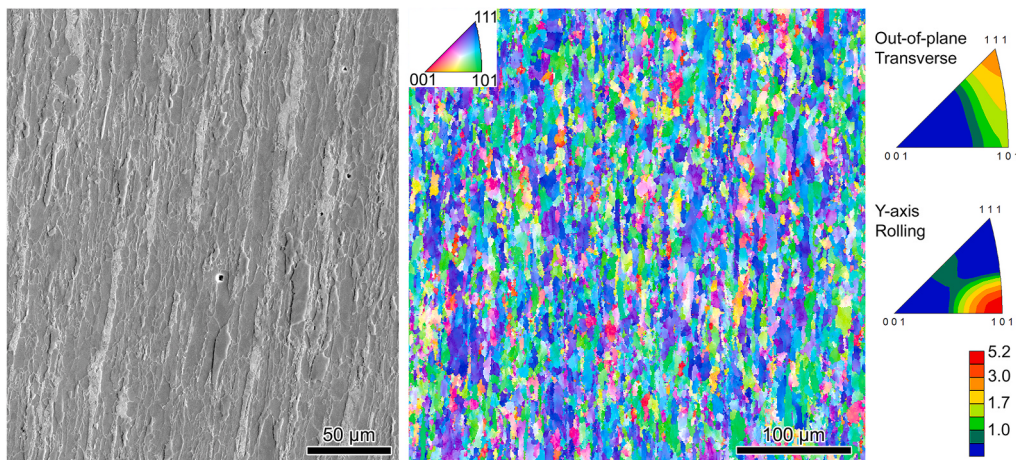


Fig. 2. SEM imaging and EBSD mapping of TD plane microstructure. (Rolling direction is \sim y-axis of image.) Grains are elongated in rolling direction. Pearlite grains (lighter grains) are thin and elongated. Strong $<111>$ texture in TD (out-of-plane) direction with a weaker $<110>$ component. Strong $<101>$ rolling (in-plane) texture. Note: While the y-axis inverse pole figure only shows the y-axis component of the grains measured in the TD plane and not the z-axis of the RD plane, in this case, it is representative of the RD plane.

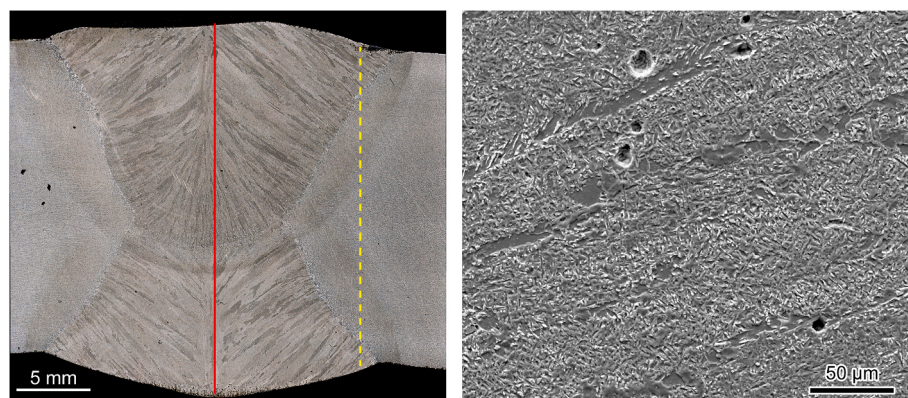


Fig. 3. Macro- and microstructure of seam weld. Optical image of weld cross-section on left. The red line indicates the approximate position of the crack plane in the “weld” specimens. The dashed yellow line indicates the approximate position of the crack in the “HAZ” specimens. Crack front propagation is into the page (Longitudinal/RD direction, along TD plane). SEM image of weld bead material on right. Etched with 2% nital.

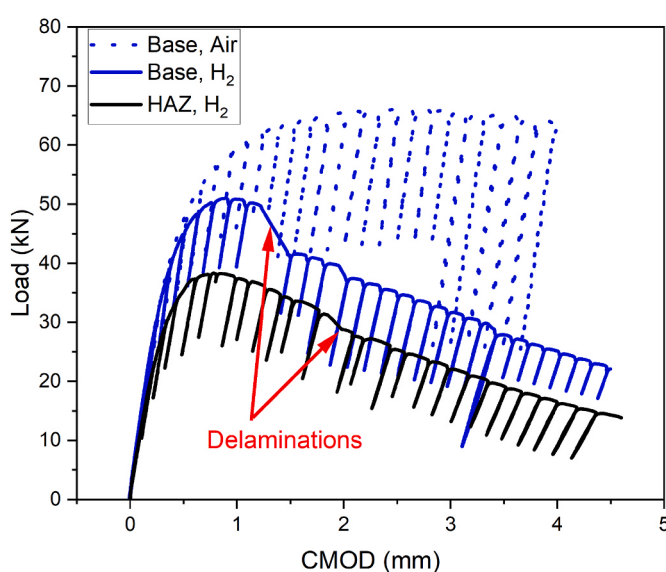


Fig. 4. Force vs CMOD curves of base metal in air and in hydrogen and of HAZ in hydrogen.

3. Results

3.1. Fracture toughness

Relationships between the force and CMOD during the fracture toughness tests of the base metal in air, the base metal in 10 MPa hydrogen gas, and the HAZ in 10 MPa hydrogen gas are shown in Fig. 4. A lower maximum force is observed for both the base metal and the weld tested in hydrogen gas compared to the base metal in air. Further, the CMOD at which the maximum force is reached is decreased due to hydrogen, from approximately 2.45 mm in air to approximately 0.9 mm in H_2 . For the two tests in hydrogen gas, the CMOD at which the maximum force is reached are roughly the same, however the maximum force was higher for the base metal compared to the HAZ (51 vs 38 kN). A noticeable step in the force vs. CMOD data was observed for the base metal tested in hydrogen, where the force decreased significantly and the CMOD increased, starting at a CMOD of approximately 1.2 mm. This may be due to delaminations, which were observed in both the base metal and HAZ fracture surfaces for the specimens tested in hydrogen gas, Fig. 5. A delamination in this case is a secondary crack that is perpendicular to the primary crack plane. A similar step was observed at a CMOD of approximately 1.75 mm for the HAZ material, though the magnitude of the force drop was significantly smaller than for the base metal. A delamination is also observed in the fracture surface of the base metal tested in air; however this delamination did not occur during the fracture toughness test, during which the crack grew only \sim 1.3 mm. Rather, the delamination occurred during the fast fracture performed

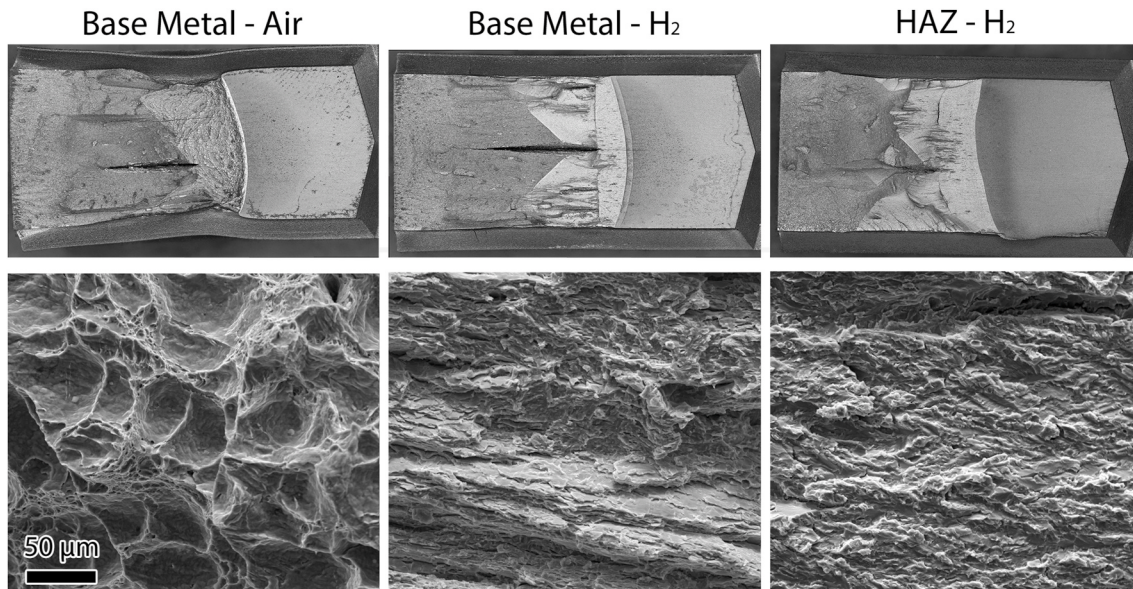


Fig. 5. Optical (top row) and SEM (bottom row) images of fracture toughness specimens. The large horizontal cracks in the fracture surfaces (top row) are delaminations. Note that the delamination in the Base Metal – Air specimen occurred during the fast-fracture process after the test to expose the fracture surface.

after the test to expose the fracture surface. Therefore, the data for the base metal in air in Fig. 4 do not show a similar feature as the data for the tests in hydrogen. However, the large number of complicated features, including multiple delaminations and evidence of crack arrest events, on the base metal in H_2 surfaces make it difficult to ascertain for certain that the delaminations are the cause, or sole cause, of the force drops.

In Fig. 5, it can be seen that the base metal tested in air shows significantly more ductility than either of the materials tested in H_2 gas. There is a significant necking of the specimen around the region of primary cracking, which is absent in the H_2 -tested specimens, as well as a more matte or darker grey-scale finish to the cracking region itself, compared to the brighter finish on the H_2 -tested specimens. Looking at the fracture features in air, the material clearly failed by ductile microvoid coalescence. In hydrogen, the fracture surfaces display flatter and brittle-appearing transgranular features.

Fig. 6 shows representative J- Δa curves for the base metal in air, the base metal in 10 MPa hydrogen gas, and the HAZ in 10 MPa hydrogen

gas. J_Q is determined as the intersection of the J- Δa fit curves with the 0.2 mm offset line, also called the “construction line”, where the J- Δa data points between the 0.15 mm offset line and the 1.5 mm offset line were used in the regression analysis to determine the fit curves. The J_Q under each condition is compared in the bar chart in Fig. 7. The base metal in air clearly has a significantly higher J_Q ($675 \pm 20 \text{ kJ/m}^2$) compared to either material in 10 MPa hydrogen. The HAZ and base metal J_Q in 10 MPa hydrogen are similar, though the base metal has a slightly higher J_Q ($38 \pm 6 \text{ kJ/m}^2$ in the base metal compared to $31 \pm 8 \text{ kJ/m}^2$ in the HAZ). Consistent with fractography, Fig. 5, the high J_Q in air indicates a huge amount of plastic deformation near the crack tip without associated crack growth, while the hydrogen embrittled steel had significantly less plastic deformation as the crack extended.

3.2. Fatigue

Fig. 8 shows the FCGR test results for the base and weld metals tested in hydrogen as a function of crack tip stress intensity factor (ΔK), the change in crack tip stress intensity factor. The plot also shows the

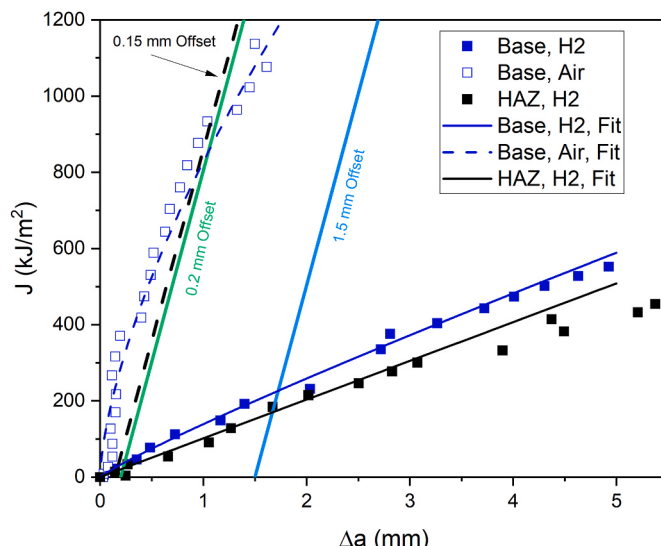


Fig. 6. J- Δa curves for base metal in air and in hydrogen and of HAZ material in hydrogen.

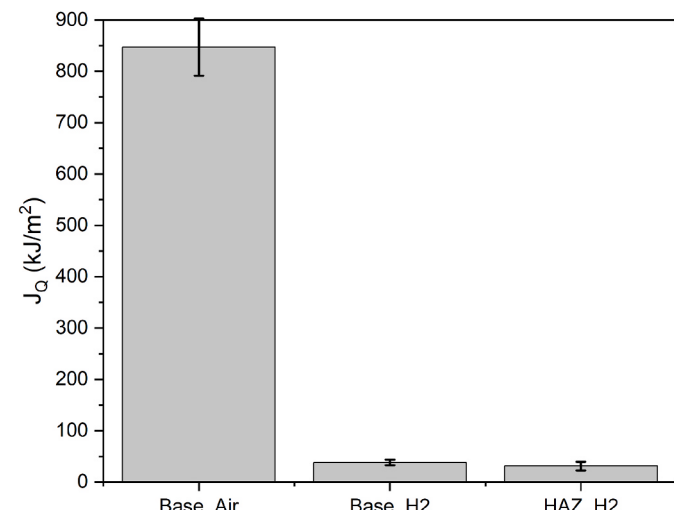


Fig. 7. Fracture toughness values of base metal in air and in hydrogen gas, and of HAZ material in hydrogen gas.

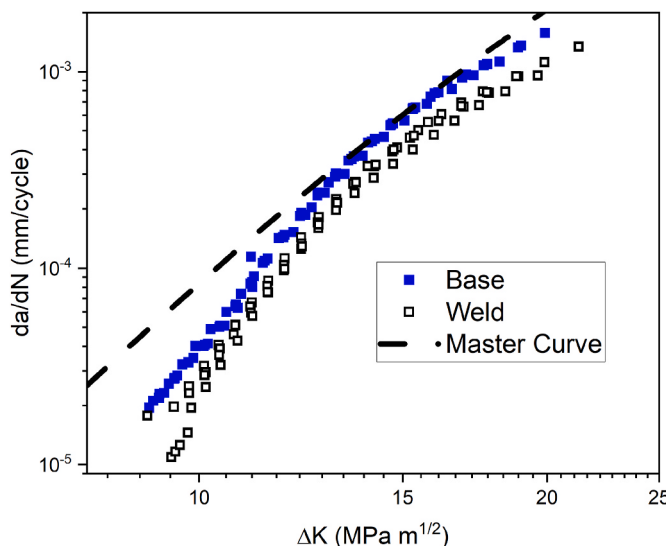


Fig. 8. FCGR curves of base and weld metal and the “Master Curve” from (Hydrogen Piping and, 2020). Note that both the Base and Weld data sets encompass results from four simultaneously run tests.

“Master Curve”, from the ASME B31.12 standard (Hydrogen Piping and, 2020). Note that the points in Fig. 8 include data encompassing all four tests of the base and all four tests of the weld. In general, for both the weld and base material, the FCGR increases with ΔK , spanning from $\sim 10^{-5}$ mm/cycle when ΔK is ~ 10 MPa m^{1/2} to $\sim 10^{-3}$ mm/cycle when ΔK is ~ 20 MPa m^{1/2}. At ΔK of approximately 12 MPa m^{1/2}, there is a clear “knee” in the data where the log-log plot is observed to transition from a higher to a lower slope. For all measured ΔK , the FCGR for both the weld and base metal is below the Master Curve. For comparison, in-air data of another X70 steel spanned $\sim 5 \times 10^{-6}$ to $\sim 5 \times 10^{-5}$ mm/cycles over the same ΔK range (Slifka et al., 2014b). The difference between the literature in-air and this study’s H₂ curves varies from half the FCGR rate at the lower $\Delta K = 10$ MPa m^{1/2} range, to nearly 2 orders of magnitude slower crack propagation at the higher $\Delta K = 20$ MPa m^{1/2} range.

In addition to the lower FCGR the weld, there is also a larger spread in measured FCGR between specimens of the weld material compared to the base metal. Both effects may be due to residual stresses within the weld region, as well as differences between the microstructure of the base metal and the weld. Compressive residual stresses can be found near welds, as the residual stress profile is often highly complicated (Ronevich et al., 2018a). The effect of these compressive residual stresses has been modeled as a change in effective R ratio due to a change in effective stress intensity factor K (Ronevich et al., 2018a). However, for the purposes of this paper we have not accounted for this change in effective R from the applied R . Qualitatively, compressive residual stresses are consistent with the observed decrease in FCGR in the weld compared to in the base material. Further, the residual stresses can vary across the pipe, which is consistent with the additional variability observed in the weld specimens compared to the base material specimens.

4. Discussion

Fracture toughness results for the base metal results show a dramatic reduction in toughness in the presence of hydrogen. At the same time, the fracture mode changes from ductile microvoid coalescence to a flatter brittle-appearing mode. This is expected for a ferritic pipeline steel. The fracture toughness in hydrogen closely matches that observed for other high strength low alloy (HSLA) pipeline steels (Stalheim et al., 2010). While the fracture features do not exactly resemble features

frequently labeled “quasi-cleavage” in the literature (Martin et al., 2011; Neeraj et al., 2012), this may be due in part to the strong rolled texture of the microstructure, as well as the presence of pearlite banding. The fracture features in the HAZ tested in hydrogen more closely resemble these more classic “quasi-cleavage” features, which may be due to recrystallization effects in the HAZ that remove or reduce the strong texture.

A potential large influence on the fracture behavior of this material is the presence of delaminations during failure. There are multiple delaminations present, particularly in the base metal specimen, but the largest delaminations in the specimens appear close to what would be the mid-line of the steel plate. This suggests these secondary cracks initiate at inhomogeneities in the microstructure, such as is commonly associated with the mid-line of a steel plate. The smaller delaminations may have initiated at features resulting from the banded microstructure. Delaminations of this sort have been previously observed during fracture toughness testing in hydrogen (San Marchi et al., 2011).

This steel was designed and deployed for natural gas transportation; it was not designed for gaseous hydrogen service. As such, certain aspects, such as the carbon content, do not satisfy the stringent recommendations in place for hydrogen service by standards codes such as ASME B31.12. It is an open question whether steel pipelines designed for natural gas can withstand the addition of 5%–10% hydrogen. While adding the requirement for new natural gas pipelines to be constructed according to the ASME B31.12 standard is possible, it may be too stringent and expensive to be feasible, and does not address the issue of using the current pipeline system. There is also the question of whether or not such demanding requirements are necessary. Some studies looking at partial pressures of hydrogen in an inert gas have shown that only small amounts (<5 vol%) are needed to observe a dramatic hydrogen effect (Meng et al., 2017; Chandra et al., 2021). However, impurities such as oxygen are able to mitigate the effect of hydrogen in concentrations of only tens of parts per millions (Someday et al., 2013; Briottet and Ez-Zaki, 2018; Ronevich et al., 2018b), including causing a transition back to ductile failure modes. Natural gas is likely to include plenty of impurities that influence the hydrogen cracking behavior. As such, testing in pure hydrogen is an extreme case, representing the most conservative position. And this steel performed well in fatigue, falling below the Master Curve (Hydrogen Piping and, 2020). The fracture toughness does decrease significantly in hydrogen, however both the base metal and HAZ had a fracture toughness ($K_{JQ} = \sqrt{\frac{E}{(1-\nu)}J_Q} = 95$ MPa m^{1/2} and 86 MPa m^{1/2}, respectively) in hydrogen above the recommended minimum (55 MPa m^{1/2}) outlined in ASME B31.12. As such, the performance of this X70 with a natural gas blended with low percentages of hydrogen gas may be acceptable, as may be the case for several steels currently in service as extant pipelines. While further studies are needed to fully define the impact of all impurities within natural gas, as opposed to laboratory methane gas, as well as determining the relationship between pipeline microstructure and hydrogen performance, these sorts of datasets will allow standard developing organizations and governing bodies to make the proper assessment prior to greenlighting blending.

5. Conclusions

Base metal and weld metal specimens sectioned from an X70 grade pipeline designed for natural gas service were tested in high pressure hydrogen to evaluate its suitability for blended natural gas/hydrogen gas service. Hydrogen had a notable impact on the fracture toughness, but the fracture toughness and fatigue behavior were within acceptable bounds for hydrogen service. The fatigue crack growth rate data fell below the Master Curve which delineates the limit of acceptable bounds for performance in hydrogen, and it was worth noting that these measurements were conducted identically to those which created the Master Curve. While it is beyond the purview of the authors to make

recommendations on acceptable usage for this steel, these sorts of datasets are critical for evaluating the feasibility of hydrogen/natural gas blending in existing natural gas pipeline systems. Given the data in the literature showing that the addition of hydrogen to an environment decreases a steel's mechanical performance until reaching a bound of behavior defined in a pure hydrogen environment, if a material is certified for H₂ service, then it should be suitable for blended natural gas/H₂ service as well. And while it is not feasible that the steel of every extant pipeline can be tested in a hydrogen environment, a comparison to steels in the literature tested in hydrogen with similar properties and microstructure may give information as to the suitability of these pipelines for blended service.

Credit author statement

May L. Martin – Investigation, Writing – Original Draft, Writing – Review & Editing, Visualization, Matthew Connolly – Conceptualization, Methodology, Formal Analysis, Investigation, Writing – Review & Editing, Zachary N. Buck – Investigation, Formal Analysis, Peter E. Bradley – Resources, Investigation, Damian Lauria – Software, Formal Analysis, Data Curation, Andrew J. Slifka – Methodology, Supervision, Conceptualization, Funding acquisition.

Declaration of competing interest

The authors declare that they have no known competing financial interests or personal relationships that could have appeared to influence the work reported in this paper.

Acknowledgements

The authors gratefully acknowledge E. Lucon at National Institute of Standards and Technology for helpful discussions on the calculation of the fracture toughness values.

Official contribution of the National Institute of Standards and Technology; not subject to copyright in the United States.

References

- Briottet, L., Ez-Zaki, H., 2018. Influence of hydrogen and oxygen impurity content in a natural gas/hydrogen blend on the toughness of an API X70 steel. In: ASME 2018 Pressure Vessels and Piping Conference.
- Chandra, A., Thodla, R., Prewitt, T.J., Matthews, W., Sosa, S., 2021. Fatigue crack growth study of X70 line pipe steel in hydrogen containing natural gas blends. In: ASME 2021 Pressure Vessels & Piping Conference.
- Collaboration between the United States and the Netherlands Focuses on Hydrogen Technology, 2020. US Department of Energy, Office of Energy Efficiency & Renewable Energy.
- Dadfarnia, M., Nibur, K.A., San Marchi, C.W., Sofronis, P., Somerday, B.P., Foulk, I., James, W., Hayden, G.A., 2010. Measurement and Interpretation of Threshold Stress Intensity Factors for Steels in High-Pressure Hydrogen Gas. <https://doi.org/10.2172/993303> (United States).
- US Dept. Of Energy, HyBlend: Opportunities for Hydrogen Blending in Natural Gas Pipelines, 2021. <https://www.energy.gov/sites/default/files/2021-08/hyblend-tech-summary.pdf>.
- Drexler, E.S., McColskey, J.D., Dvorak, M., Rustagi, N., Lauria, D.S., Slifka, A.J., 2016. Apparatus for accelerating measurements of environmentally assisted fatigue crack growth at low frequency. *Exp. Tech.* 40, 429–439.
- ASME, 2020. Hydrogen Piping and Pipelines B31.12-2019.
- Martin, M.L., Robertson, I.M., Sofronis, P., 2011. Interpreting hydrogen-induced fracture surfaces in terms of deformation processes: a new approach. *Acta Mater.* 59, 3680–3687.
- Martin, M.L., Connolly, M.J., DelRio, F.W., Slifka, A.J., 2020. Hydrogen embrittlement in ferritic steels. *Appl. Phys. Rev.* 7, 041301.
- Melaina, M.W., 2016. Market transformation lessons for hydrogen from the early history of the manufactured gas industry. In: Grasman, S.E. (Ed.), *Hydrogen Energy and Vehicle Systems*. CRC Press, pp. 123–155.
- Melaina, M.W., Antonia, O., Penev, M., 2013. Blending Hydrogen into Natural Gas Pipeline Networks: A Review of Key Issues. National Renewable Energy Lab. (NREL), Golden, CO (United States). <https://doi.org/10.2172/1068610>.
- Meng, B., Gu, C., Zhang, L., Zhou, C., Li, X., Zhao, Y., Zheng, J., Chen, X., Han, Y., 2017. Hydrogen effects on X80 pipeline steel in high-pressure natural gas/hydrogen mixtures. *Int. J. Hydrogen Energy* 42, 7404–7412.
- Neeraj, T., Srinivasan, R., Li, J., 2012. Hydrogen embrittlement of ferritic steels: observations on deformation microstructure, nanoscale dimples and failure by nanovoiding. *Acta Mater.* 60, 5160–5171.
- Nguyen, T.T., Park, J., Kim, W.S., Nahm, S.H., Beak, U.B., 2020. Effect of low partial hydrogen in a mixture with methane on the mechanical properties of X70 pipeline steel. *Int. J. Hydrogen Energy* 45, 2368–2381.
- Nibur, K.A., Somerday, B.P., Marchi, C.S., Foulk, J.W., Dadfarnia, M., Sofronis, P., 2013. The relationship between crack-tip strain and subcritical cracking thresholds for steels in high-pressure hydrogen gas. *Metall. Mater. Trans.* 44, 248–269.
- Ronevich, J.A., Somerday, B.P., San Marchi, C.W., 2016. Effects of microstructure banding on hydrogen assisted fatigue crack growth in X65 pipeline steels. *Int. J. Fatig.* 82, 497–504.
- Ronevich, J.A., D'Elia, C.R., Hill, M.R., 2018a. Fatigue crack growth rates of X100 steel welds in high pressure hydrogen gas considering residual stress effects. *Eng. Fract. Mech.* 194, 42–51.
- Ronevich, J., San Marchi, C., Kolasinski, R., Thurmer, K., Bartelt, N., El Gabaly, F., Somerday, B., 2018b. Oxygen impurity effects on hydrogen assisted fatigue and fracture of X100 pipeline steel. In: ASME 2018 Pressure Vessels and Piping Conference.
- San Marchi, C., Somerday, B.P., Nibur, K.A., Stalheim, D.G., Boggess, T., Jansto, S., 2010. Fracture and fatigue of commercial grade API pipeline steels in gaseous hydrogen. In: ASME 2010 Pressure Vessels and Piping Division/K-PVP Conference, pp. 939–948.
- San Marchi, C., Somerday, B.P., Nibur, K.A., Stalheim, D.G., Boggess, T., Jansto, S., 2011. Fracture resistance and fatigue crack growth of X80 pipeline steel in gaseous hydrogen. In: ASME Pressure Vessels and Piping Conference 2011. ASME, Baltimore, US, pp. 841–849.
- Slifka, A.J., Stalheim, D.G., 2021. Personal Communication.
- Slifka, A.J., Drexler, E.S., Nanninga, N.E., Levy, Y.S., McColskey, J.D., Amaro, R.L., Stevenson, A.E., 2014a. Fatigue crack growth of two pipeline steels in a pressurized hydrogen environment. *Corrosion Sci.* 78, 313–321.
- Slifka, A.J., Drexler, E.S., Amaro, R.L., Lauria, D.S., Hayden, L.E., Stalheim, D.G., Chen, Y., 2014b. Summary of an ASME/DOT project on measurements of fatigue crack growth rate of pipeline steels. In: ASME 2014 Pressure Vessels and Piping Conference.
- Slifka, A.J., Drexler, E.S., Amaro, R.L., Lauria, D.S., Hayden, L.E., McCowan, C.N., Sowards, J.W., 2015. Measurements of fatigue crack growth rates of the heat-affected zones of welds of pipeline steels. In: ASME 2015 Pressure Vessels and Piping Conference.
- Somerday, B.P., Sofronis, P., Nibur, K.A., San Marchi, C., Kirchheim, R., 2013. Elucidating the variables affecting accelerated fatigue crack growth of steels in hydrogen gas with low oxygen concentrations. *Acta Mater.* 61, 6153–6170.
- Stalheim, D., Boggess, T., San Marchi, C., Jansto, S., Somerday, B., Muralidharan, G., Sofronis, P., 2010. Microstructure and mechanical property performance of commercial grade API pipeline steels in high pressure gaseous hydrogen. In: 2010 8th International Pipeline Conference, pp. 529–537.
- E647-15 Standard Test Method for Measurement of Fatigue Crack Growth Rates ASTM, 2017. ASTM, West Conshohocken, PA.
- Standard Test Method for Measurement of Fracture Toughness ASTM E1820-20b, 2019. ASTM, West Conshohocken, PA.